Full waveform inversion for ultrasonic flaw identification

Robert Seidl and Ernst Rank

Citation: AIP Conference Proceedings **1806**, 090013 (2017); doi: 10.1063/1.4974657
View online: http://dx.doi.org/10.1063/1.4974657
View Table of Contents: http://aip.scitation.org/toc/apc/1806/1
Published by the American Institute of Physics

Full Waveform Inversion for Ultrasonic Flaw Identification

Robert Seidl[1, a)] and Ernst Rank[1, 2, b)]

[1]*Chair for Computation in Engineering, Faculty of Civil, Geo and Environmental Engineering, Technical University of Munich, Arcisstrasse 21, 80333 Munich, Germany*
[2]*Institute for Advanced Study, Technical University of Munich, Germany*

[a)]Corresponding author: robert.seidl@tum.de
[b)]ernst.rank@tum.de

Abstract. Ultrasonic Nondestructive Testing is concerned with detecting flaws inside components without causing physical damage. It is possible to detect flaws using ultrasound measurements but usually no additional details about the flaw like position, dimension or orientation are available. The information about these details is hidden in the recorded experimental signals. The idea of full waveform inversion is to adapt the parameters of an initial simulation model of the undamaged specimen by minimizing the discrepancy between these simulated signals and experimentally measured signals of the flawed specimen. Flaws in the structure are characterized by a change or deterioration in the material properties. Commonly, full waveform inversion is mostly applied in seismology on a larger scale to infer mechanical properties of the earth. We propose to use acoustic full waveform inversion for structural parameters to visualize the interior of the component. The method is adapted to US NDT by combining multiple similar experiments on the test component as the typical small amount of sensors is not sufficient for a successful imaging. It is shown that the combination of simulations and multiple experiments can be used to detect flaws and their position, dimension and orientation in emulated simulation cases.

INTRODUCTION

Ultrasonic Nondestructive Testing (US NDT) is based on the propagation of low amplitude waves through the material, measuring the travel time and intensity of the waves at specific sensors. In the conventional approach these physical measurements – or some selected features – are compared to reference measurements of the flawless specimen by a human expert who then decides if a flaw in the specimen is to be expected or not. This is shown in Figure 1. Following this approach it is possible to detect damage - but usually not to provide detailed information on the damage parameters. Recently this approach has been extended by considering numerical time-reversal simulations. (Givoli, 2014)

Full waveform inversion has been widely and very successfully used in seismology in the last ten years. The method was known already in the 1980's (Tarantola, 1984) but only the recent advances in computing power and storage allow to solve the demanding problems in seismology where it is necessary to invert for multiple parameters in complex earth models. (Fichtner et al., 2013; Virieux and Operto, 2009) Because the method is able to image the interior of the earth in great detail using measurements of earthquake waves, the idea to adapt the methodology to the smaller scale of US NDT seems plausible and promising. In a certain way full waveform inversion extends the common US NDT approach by adding an adaptable simulation model of the healthy specimen instead of the fixed reference measurements. Such a model might be available through an initial CT scan or a CAD model. The idea is to adapt the simulation model, or more precisely its parameters like the wave speed of pressure or shear waves inside the specimen, in an iterative fashion such that in the end the simulation model itself is able to generate signals at the sensors that are similar to the physical measurements. This approach is depicted in Figure 2. As result, the adapted simulation model can be used to perform an image based investigation of flaws or inclusions. The method is very general and can have multiple applications in US NDT ranging from the simultaneous detection of multiple cracks or flaws of different sizes to material or flaw characterization. The goal of this publication is to present the method in the

43rd Annual Review of Progress in Quantitative Nondestructive Evaluation, Volume 36
AIP Conf. Proc. 1806, 090013-1–090013-7; doi: 10.1063/1.4974657
Published by AIP Publishing. 978-0-7354-1474-7/$30.00

simplest acoustic setting and to provide some examples how the method could be applied in the context of US NDT. One recent example where full waveform inversion already showed to be very promising is in the context of guided wave imaging of corrosion in tubes by (Rao et al., 2016).

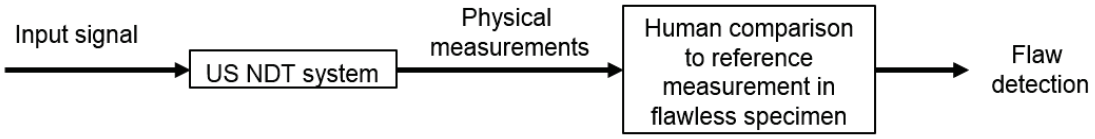

FIGURE 1. Standard NDT system

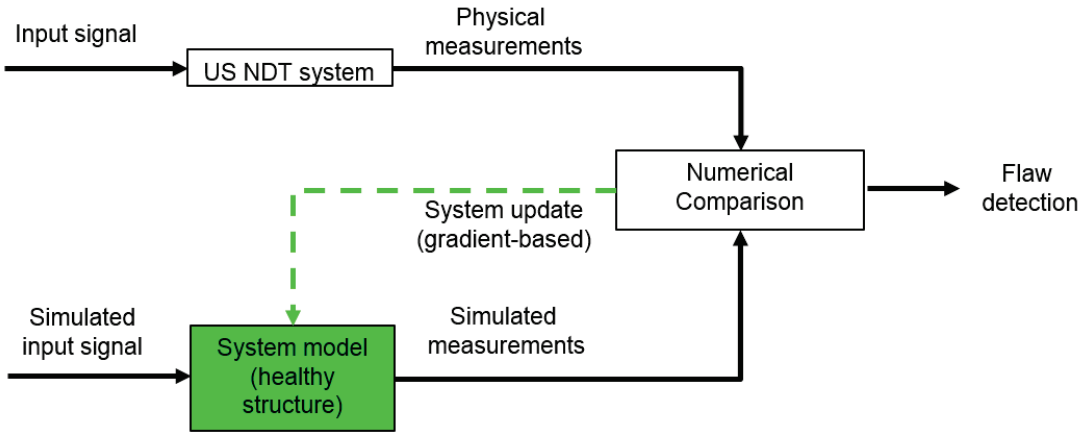

FIGURE 2. Simulation model based NDT system

METHOD

The idea of full waveform inversion is to use the discrepancy between experimentally measured ultrasonic signals that include information about possible flaws and inclusions and computed signals from a simulation model of the undamaged structure to adapt the wave speed of the simulation model iteratively such that in the end the simulation model is able to generate the experimental signals. If this is the case the adapted wave speed distribution in the final simulation model should present information about the flaws in the structure. It can be inspected visually for possible flaws and inclusions. Even though a similar approach can be used for elastic wave propagation, we present the method in the context of acoustic wave propagation for two reasons. First, the derivation of the method is simplified significantly in the simpler acoustic case and second, there is no ambiguity in the interpretation of the results of the inversion as the output is a scalar speed map. For more information about using an elastic model instead see (Pratt et al., 1998; Tromp et al., 2008; Virieux and Operto, 2009)

The wave propagation of pressure waves induced by an applied ultrasonic impulse in a two- or three-dimensional medium Ω for a time span of T (micro) seconds, is modeled by the acoustic wave equation

$$\frac{\partial^2 u(x,t)}{\partial t^2} - v_p^2(x)\Delta u(x,t) = f_s(x,t) \;\; for\; x \in \Omega \subset \mathbb{R}^2 \; or \; \mathbb{R}^3, t \in [0,T] \tag{1a}$$

$$u(x,t) = u_t(x,t) = 0 \; on \; \Omega \tag{1b}$$

$$u = 0 \; on \; \partial\Omega. \tag{1c}$$

All boundaries are assumed to be rigid. Here, $v_p(x)$ is the propagation speed of the pressure waves in the material. It is assumed to be piecewise constant on a fine enough predefined grid that is able to represent the flaw. The ultrasonic impulse f_s is modeled as a point source, $f_s = A(t) \cdot \delta(x - x_s)$, where x_s is the source position and $A(t)$ is the time-varying amplitude of the source. The solution is measured at n distinct sensor locations $x_i^r, i = 1, \dots, n$.

This model is used together with the setup of the experiment to generate comparable signals at the sensor locations. To measure the discrepancy between these signals and the experimental signals of the flawed structure, we formulate the following least-squares functional

$$\chi(\boldsymbol{m}) = \int_{\Omega}\int_{T}\frac{1}{2}\sum_{i=1}^{N}[u(m;x,t) - u^0(x,t)]^2\delta(x - x_i^r)dt\,dx\,. \tag{2}$$

It is often called cost or misfit functional. Here $u(m;x,t)$ is the simulated wavefield that is defined implicitly as solution to the acoustic wave equation (1). $u^0(x,t)$ are the experimental signals that are only measured at n distinct sensor locations x_i^r. The Dirac δ function is used to account for this pointwise comparison. The functional is depending on a set of model parameters $\boldsymbol{m} \coloneqq v_p^2(x)$. As the wave propagation speed is a distributed parameter on a possibly very fine grid, this results in a large amount of parameters that have to be adapted. In our simulations the number of parameters are in the order of $O(10^4)$ to $O(10^6)$ for the inverse acoustic problem for 2D and 3D problems respectively. Supposed the measured signals from the flawed specimen and the simulated signals agree, then the cost function is zero. If there is a discrepancy between the signals then its value is larger than zero and quantifies the misfit between the signals. Therefore, the goal is to minimize $\chi(m)$ with respect to the large amount of model parameters. Clearly, global optimization methods are not suitable in this case because the acoustic wave equation has to be solved for each evaluation of $\chi(m)$. Therefore, one has to use a local optimization method that tries to decrease the nonlinear misfit function step by step until it ends up in a local minimum. We use a simple steepest descent method. Given the actual model $\boldsymbol{m}_i$, it is improved by employing the following update:

$$\boldsymbol{m}_{i+1} = \boldsymbol{m}_i + \gamma_i \boldsymbol{h}_i. \tag{3}$$

Here, h_i is a descent direction of χ, and γ_i is a step size that fulfills $\chi(\boldsymbol{m}_{i+1}) < \chi(\boldsymbol{m}_i)$. In the case of steepest descent, the negative gradient is chosen as a suitable direction.

$$h_i = -\nabla_m \chi(\boldsymbol{m}). \tag{4}$$

The most delicate part of the algorithm is the computation of $\nabla_m \chi(\boldsymbol{m})$ because of the dependence on the large amount of model parameters $\boldsymbol{m}$. The gradient of the cost function with respect to $\boldsymbol{m}$ is derived by applying the chain rule.

$$\nabla_m \chi = \int_{\Omega}\int_{0}^{T}\sum_{i=1}^{N}[u(m;x,t) - u^0(x,t)]\delta(x - x_i^r)\cdot\frac{\partial u}{\partial \boldsymbol{m}}dt\,dx \tag{5}$$

The sensitivity $\frac{\partial u}{\partial \boldsymbol{m}}$ poses a serious computational challenge as it would have to be computed for each model parameter in $\boldsymbol{m}$. A naive approximation of this gradient by finite differences would need at least $N+1$ evaluations of $\chi(m)$. This is clearly impractical as each evaluation requires the solution of the acoustic wave equation.
As shown in (Fichtner, 2011; Seidl and Rank, 2016) the gradient can be efficiently computed using an adjoint formulation of equation (5) by

$$\nabla_m \chi = \int_{\Omega}\int_{0}^{T}\Delta u \cdot u^{\dagger} dt\,dx\,. \tag{6}$$

Here, $u^{\dagger}$ is the solution of the following adjoint equation:

$$\frac{\partial^2 u^{\dagger}(x,t)}{\partial t^2} - v_p^2(x)\Delta u^{\dagger}(x,t) = f_s^{\dagger}(x,t)\ \ for\ x \in \Omega \subset \mathbb{R}^2\ or\ \mathbb{R}^3, t \in [0,T] \tag{7a}$$

$$u^{\dagger}(x,T) = u_t^{\dagger}(x,T) = 0\ on\ \Omega \tag{7b}$$

$$u^{\dagger} = 0\ on\ \partial\Omega, \tag{7c}$$

where the adjoint source is given by $f_s^{\dagger}(x,t) \coloneqq \sum_{i=1}^{N}[u(m;x,t) - u^0(x,t)]\delta(x - x_i^r)$.

The adjoint equation is very similar to equation (1) (called the *forward* problem) with two important differences. It is solved backwards in time because of the terminal conditions and its source is a distributed point source: the time-reversed residual between computed sensor signals and experimental data at the sensor locations. Given the solution of the adjoint equation the calculation of the gradient simplifies significantly. Now, one forward and one adjoint solution suffice to calculate the gradient with respect to all model parameters. For more details about adjoint equations see (Hinze, 2009; Marchuk, 1995). After the gradient is computed the step size can be obtained by a line search or more advanced techniques as described in (Nocedal and Wright, 1999). Then the model parameters are updated using equation (3). This process is repeated until a local minimum is reached.

APPLICATIONS

To see the benefits of the proposed inversion method it is applied to detect flaws in a three-dimensional homogeneous block by imaging the interior of the object. In a second example a strongly inhomogeneous two-dimensional model of a human femur is used to show the applicability to more complex and inhomogeneous structures.

The block has dimensions $10cm^3$ and a homogeneous wave speed of $v_p = 6420\ \frac{m}{s}$ inside is assumed. All boundaries are considered rigid. Experimental sensor data is emulated using a second simulation model, where three flaws, two horizontal flaws on top of each other and one vertical flaw, are modeled as small regions where the wave speed model deviates from the background wave speed as shown in Figure 3(a). As experimental data was not available, a smaller wave speed is assumed for the flaws, modeled by $v_f = 0.7v_p$ and this data is emulated using a second simulation. In both cases the propagation of pressure waves is modeled by the acoustic wave equation (1) and ultrasonic point sources are applied on the boundaries one at a time to scan the specimen from different angles. In all cases the ultrasonic source is modeled as a Ricker wavelet pulse with a dominant frequency f_0:

$$f_s(x,t) = f_0^2 \cdot (t - t_0) \cdot \exp(-f_0^2 \cdot (t - t_0)^2) \cdot \delta(x - x_0), \tag{8}$$

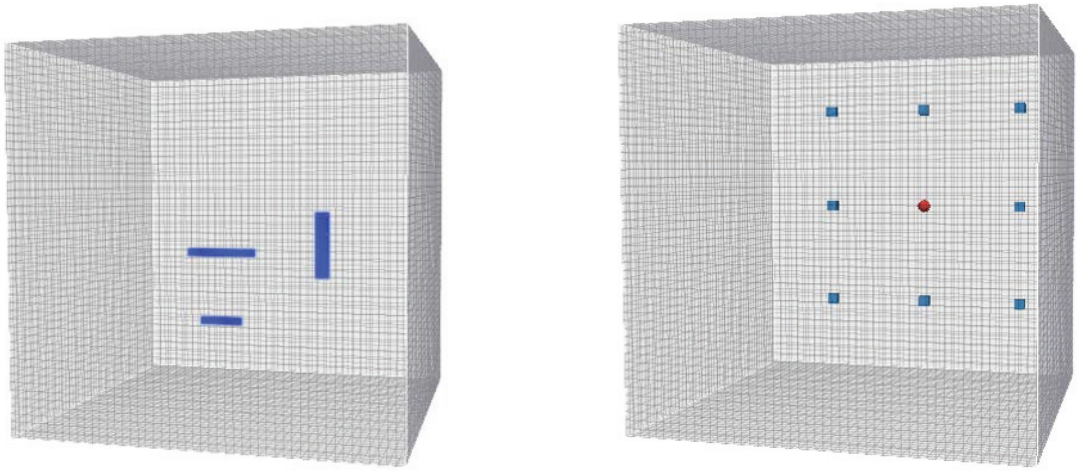

(a) experimental model (b) initial simualtion model

FIGURE 3. Unknown experimental model and setup of sensors (blue box) and source (red circle) at one face.

where t_0 is the delay and x_0 the position where the point source is applied. The wave propagation of the pulse is modeled for a time span of $48\ \mu s$. The forward and adjoint acoustic wave equations are solved using finite differences in space and time with accuracy orders of $O(\Delta x^4)$ and $O(\Delta t^2)$. The spatial discretization of the block is one grid point per two millimeter. It is chosen fine enough to be able to resolve different flaws. Simulation time and time step size are chosen such that the CFL condition is satisfied, a smooth source signal is generated and the wave form moves at least once through the complete domain. Because the same grid is used for the solution of the wave equation and the model parameter, i.e. the speed of the pressure waves, the discretization results in 125 000 model parameters which are updated simultaneously each step by the inversion process.

Furthermore, the cost function is adapted to handle data from multiple experiments where the same source is applied at k different positions, as this is the common case in NDT.

$$\chi(\boldsymbol{m}) = \int_\Omega \int_0^T \frac{1}{2} \sum_{k=1}^{K} \sum_{i=1}^{N} [u(m, s_k; x, t) - u^0(s_k; x, t)]^2 \delta(x - x_i^r)\, dt\, dx \tag{9}$$

As a result k simulations need to be performed to evaluate the cost function once and $2K$ simulations for evaluating the gradient. (Seidl and Rank, 2016) showed that scanning the structure and its flaws from different angles greatly improves the results of the inversion. Figure 3(b) shows the placement of sensors and source for the back face of the

block. Eight sensors are placed at each face for a total of 64 sensors, and the same source is applied at the midpoint of each face once resulting in six experiments. Steepest descent is run for 30 iterations until a local minimum is found. Figure 4 gives a visual comparison of the experimental structure being unknown at the beginning of the simulation and the inverted structure from different angles. A homogeneous block is assumed in the beginning of the inversion. The structure can be clearly identified as 'damaged' by a visual inspection. Moreover, the position, dimension and orientation of all three flaws is clearly visible.

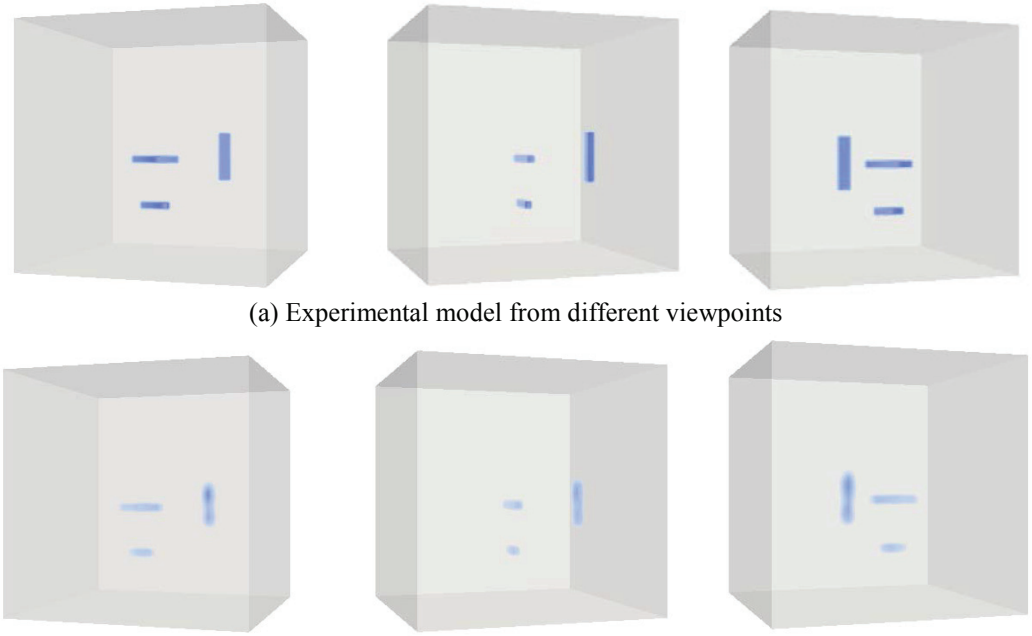

(a) Experimental model from different viewpoints

(b) Inverted model from different viewpoints

FIGURE 4. Comparison of experimental and inverted model

The inversion approach is general and not limited to simple and homogeneous structures. To show these further benefits it is applied to a more complex model of the human femur. The material properties, more precisely the speed of compressional waves inside the bone, and its geometry are derived from a qCT scan and empirical modeling as described in (Wille et al., 2012). For simplicity, only a two dimensional slice of the bone model is used. The strongly inhomogeneous wave speed distribution $v_p(x)$ is shown in Figure 5(a). Seven sensors, marked by black boxes, and four sources, shown as green spheres, are placed at the boundary of the bone. It has a height of 240 mm and a width of 100 mm. A discretization of 506 x 106 grid points is used which leads to around 50 000 model parameters. As source signal the same Ricker wavelet as before is used with a dominant frequency $f_s = 150\ kHz$. Again, because no lab data is available a modified simulation model is used to generate sensor measurements of a flawed structure. Here, a L-shaped flaw with a wave speed of $v_{p,flaw} = 1500\ m/s$ is introduced as shown in Figure 5(b). Steepest descent is run for 30 iterations until a local minimum was reached. Figure 6 shows the deviation from the initial bone model. The L-shaped flaw is clearly reconstructed successfully.

OUTLOOK

It has been shown how the concept of full waveform inversion can be described as model-based NDT device where an adaptable wave speed of a simulation model of the healthy structure is corrected in an iterative fashion such that the simulation model is able to generate sensor signals that are close to experimental signals of the flawed structure. As result the wave speed can be used to image flaws inside the structure. Because of the general setup of the method it can have multiple applications in US NDT ranging from simultaneous detection of multiple cracks or

flaws of different sizes to material or flaw characterization. This method was shown to work well to visualize the position and shape of emulated flaws for a complex 2D bone example and a 3D homogeneous block when using data from multiple similar experiments and a limited amount of sensors. In both cases all flaws can be determined by a visual inspection of the adapted wave speed of the simulation model. As important next steps, it is planned to validate the results by coupling the simulation method with sensor data from real acoustic experiments. Furthermore the method should be extended to use the elastic wave equation and a finite element simulation model such that it can be applied to more realistic NDT problems where for instance body waves are used to inspect a structure.

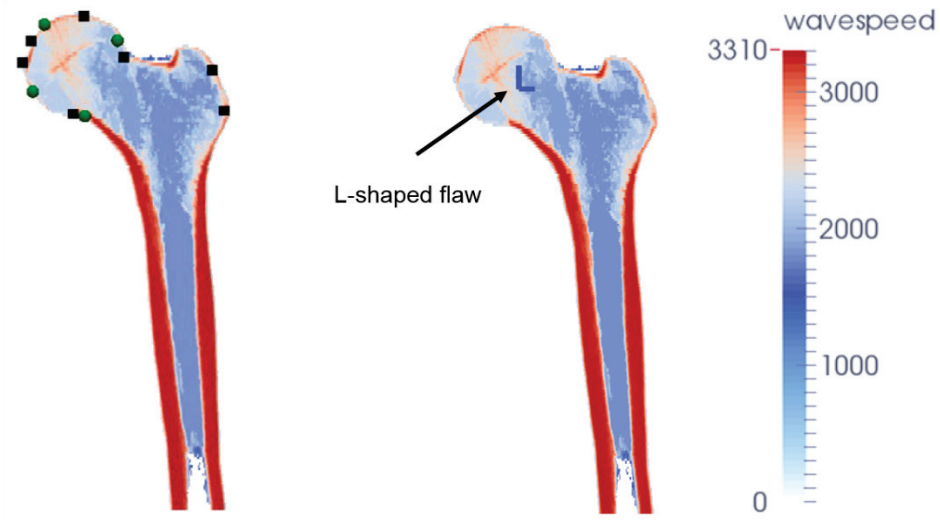

(a) Initial model (b) Experimental model

FIGURE 5. Wave speed models of human femur

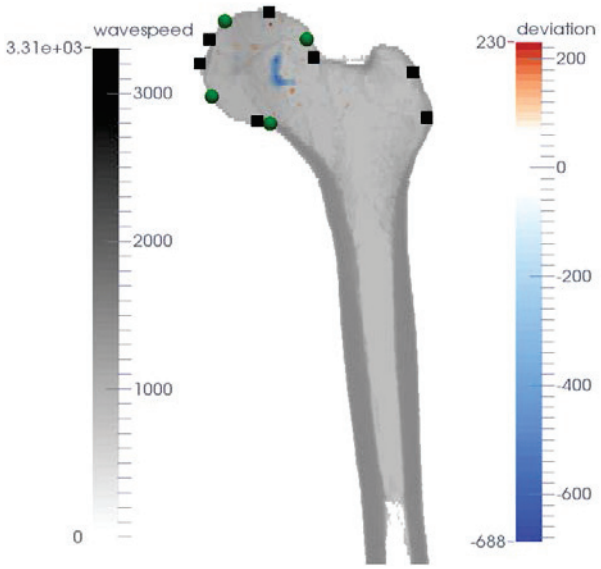

FIGURE 6. Deviation from initial model

REFERENCES

1. Fichtner, A., *Full Seismic Waveform Modelling and Inversion*, (Springer, Heidelberg, 2011).
2. Fichtner, A., Trampert, J., Cupillard, P., Saygin, E., Taymaz, T., Capdeville, Y., Villasenor, A., Multiscale full waveform inversion. Geophys. J. Int. **194**, 534–556 (2013).
3. Givoli, D., Time Reversal as a Computational Tool in Acoustics and Elastodynamics. J. Comput. Acoust. **22**, 1430001 (2014).
4. Hinze, M. (Ed.), *Optimization with PDE constraints*, (Springer, Dordrecht, 2009).
5. Marchuk, G.I., *Adjoint Equations and Analysis of Complex Systems*, (Springer, Dordrecht, 1995).
6. Nocedal, J., Wright, S.J., *Numerical optimization*, (Springer, New York, 1999).
7. Pratt, R.G., Shin, C., Hick, G.J., Gauss–Newton and full Newton methods in frequency–space seismic waveform inversion. Geophys. J. Int. **133**, 341–362 (1998).
8. Rao, J., Ratassepp, M., Fan, Z., Guided Wave Tomography Based on Full Waveform Inversion. IEEE Trans. Ultrason. Ferroelectr. Freq. Control **63**, 737–745 (2016).
9. Seidl, R., Rank, E., Iterative time reversal based flaw identification. Comput. Math. Appl. **72**, 879–892 (2016).
10. Tarantola, A., Inversion of seismic reflection data in the acoustic approximation. GEOPHYSICS **49**, 1259–1266 (1984).
11. Tromp, J., Komattisch, D., Liu, Q., Spectral-element and adjoint methods in seismology. Commun. Comput. Phys. **3**, 1–32 (2008).
12. Virieux, J., Operto, S., An overview of full-waveform inversion in exploration geophysics. GEOPHYSICS **74**, WCC1-WCC26 (2009).
13. Wille, H., Rank, E., Yosibash, Z., Prediction of the mechanical response of the femur with uncertain elastic properties. J. Biomech. **45**, 1140–1148 (2012).